Interplay Between Solid State Microstructure and Photophysics for Poly(9,9-dioctylfluorene) within Oriented Polyethylene Hosts

Interplay Between Solid State Microstructure and Photophysics for Poly(9,9-dioctylfluorene) within Oriented Polyethylene Hosts

Aleksandr Perevedentsev,[1] Seda Aksel,[2] Kirill Feldman,[2] Paul Smith,[2] Paul N. Stavrinou,[1] Donal D. C. Bradley[1]

[1]Department of Physics and Centre for Plastic Electronics, Imperial College London, SW7 2AZ, United Kingdom
[2]Department of Materials, Eidgenössische Technische Hochschule (ETH) Zürich, Wolfgang-Pauli-Strasse 10, 8093 Zürich, Switzerland
Correspondence to: D. D. C. Bradley (E-mail: d.bradley@imperial.ac.uk)

Received 22 July 2014; accepted 8 September 2014; published online 3 October 2014
DOI: 10.1002/polb.23601

ABSTRACT: We present a study of isotropic and uniaxially oriented binary blend films comprising $\leq$1 wt % of the conjugated polymer poly(9,9-dioctylfluorene) (PFO) dispersed in both ultra-high molecular weight (UHMW) and linear-low-density (LLD) polyethylene (PE). Polarized absorption, fluorescence and Raman spectroscopy, scanning electron microscopy, and X-ray diffraction are used to characterize the samples before and after tensile deformation. Results show that blend films can be prepared with PFO chains adopting a combination of several distinct molecular conformations, namely glassy, crystalline, and the so-called β-phase, which directly influences the resulting optical properties. Both PFO concentration and drawing temperature strongly affect the alignment of PFO chains during the tensile drawing of the blend films. In both PE hosts, crystallization of PFO takes place during drawing; the resulting ordered chains show optimal optical anisotropy. Our results clarify the PFO microstructure in oriented blends with PE and the processing conditions required for achieving the maximal optical anisotropy. © 2014 The Authors. Journal of Polymer Science Part B: Polymer Physics Published by Wiley Periodicals, Inc. J. Polym. Sci., Part B: Polym. Phys. **2015**, *53*, 22–38

KEYWORDS: blends; conjugated polymers; crystallization; orientation; polyethylene; polyfluorene)

INTRODUCTION Molecular semiconductors are distinct from elemental and compound inorganic semiconductors in a number of important ways. One key feature is the option of low temperature processability that derives from relatively weak (typically van der Waals) intermolecular bonding; this allows the molecules in solid form to be readily separated in solution or melt and then reassembled in, for example, films on a device substrate. It is an enabling characteristic for printable/plastic electronics and has attracted major interest since the first report of solution-processed conjugated polymer light-emitting diodes (LEDs).[1] A consequence of relatively weak inter-molecular bonding is, however, that the solid-state microstructure can be sensitive to processing conditions and, therefore, complex. As a result, a range of amorphous/glassy, liquid-crystalline (LC) and (semi-)crystalline phases are found for many conjugated polymers.

This feature has been widely documented for the prototypical fluorene-based polymer, poly(9,9-dioctylfluorene) (PFO) and, therewith, provides an excellent research space within which to explore the influence of microstructure on photophysical and other functional properties.[2–6] The solid-state structure of PFO has been reported to include "glassy," "crystalline," and "β-phase" chain conformations,[7–15] the main differences between which are shown schematically in Figure 1. Spin-coating PFO films from low boiling point solvents, such as chloroform or tetrahydrofuran, typically yields glassy films[2,11,15] that are isotropic within the plane. The corresponding chain geometry, usually also referred to as "glassy" in the literature, is worm-like with a broad distribution of intermonomer torsion angles, resulting in a featureless, inhomogeneously broadened absorption spectrum. Crystalline PFO[2,11,12] formed during crystallization from the melt possesses a more extended chain conformation, generally evidenced by a shoulder at $\sim$425 nm in the corresponding absorption spectrum, with some variation seen for different crystallization conditions. The β-phase conformation[2,7,9,10,15] refers

Additional Supporting Information may be found in the online version of this article.

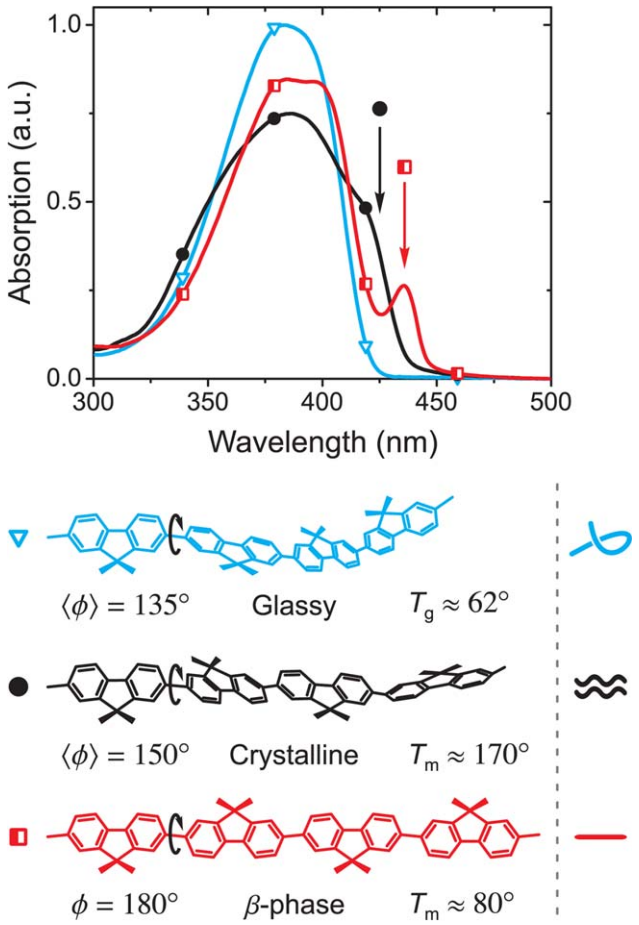

FIGURE 1 Area-normalized absorption spectra of PFO thin films in as-spin-coated glassy state (blue line + open triangles), and with crystalline (black line + filled circles), and β-phase (red line + semifilled squares) chain segment fractions introduced by the appropriate treatments (see Experimental section). The differences between the three chain conformations are presented in terms of their intermonomer torsion angle ϕ and basic thermal properties (note that the given values can vary somewhat depending on the details of film processing and polymer molecular weight). Alkyl side-chains of PFO (C_8H_{17}) are omitted for clarity. Schematic representations of the respective chain segment conformations, as used later in the manuscript, are shown in the column on the right.

to a rigid planar-zigzag chain geometry, characterized by the intermonomer torsion angle $\phi = 180°$, that can be introduced in solid-state PFO by, most commonly, exposure to moderately good solvents. The β-phase conformation is metastable[2,13,15] with a relatively low melting temperature, $T_m = 80°$; its well-defined geometry results in distinct absorption features with a sharp peak at ~435 nm. We emphasize that the different chain conformations described above can in fact be adopted by discrete chain *segments* and in a relatively high molecular weight polymer as used in this study, a single chain can contain segments possessing different conformations. While there are further subtleties to the PFO microstructural space arising from, for example, crystallization conditions,[12] macromolecular orientation[14–17] and blending with other polymers,[18–20] for the sake of clarity we will adopt the simplified nomenclature presented above and in Figure 1.

With respect to uniaxial order, direct orientation of PFO chains has been demonstrated via heating films into their thermotropic LC state on a variety of rubbed alignment layers including polyimide, poly(*p*-phenylenevinylene) and poly(3,4-ethylenedioxythiophene)/polystyrene-sulphonate.[14,15,17,21,22] Friction-transfer deposition[23,24] and directional epitaxial crystallization[25] have also been used. The resulting film structure can be controlled to be predominantly glassy (after rapid quenching from the LC melt) or crystalline (after slow cooling from the LC melt or following friction transfer and epitaxial crystallization) and β-phase chains can be subsequently generated by the usual post-deposition treatments.[15,22,26] Oriented PFO films prepared by these methods exhibit attractive properties such as improved hole mobility,[16] enhanced optical gain,[27] and anisotropic light emission with polarization ratios $\leq$50 achieved for LEDs based on oriented films.[17,26] They also demonstrate a large anisotropy in refractive index that allows highly polarized, reduced linewidth photoluminescence (PL) emission from microcavity structures.[28,29]

Another approach to achieving uniaxial chain alignment is based on incorporation of the conjugated polymer as a guest within an inert polymer matrix, followed by tensile drawing of the blend. The resulting films have proven very useful for investigations of the anisotropic aspects of conjugated polymer photophysics[30–33] and as performance enhancing, polarizing, photoluminescent color filters for LC displays.[34–36] Ultra-high molecular weight polyethylene (UHMWPE) is particularly suited as the matrix polymer for such studies as, when appropriately processed, it allows for extraordinarily high degrees of uniaxial alignment. Films of UHMWPE so-called "gel-processed" from semi-dilute solution can be easily stretched to over 100 times their original length due to the polymer's high molecular weight, absence of branches and a reduced density of entanglements.[37–39]

There have been several reports published on polyfluorenes (PFs) oriented in gel-processed blends with UHMWPE. He et al.[40] reported a maximum PL emission anisotropy of 58 from oriented samples containing 0.5 wt % of low molecular weight ($M_n = 9000$) PFO. King et al.[32] used similar blends to study the orientation of transition dipole moments for poly(9,9-bis(2-ethylhexyl)fluorene) (PF2/6) while Knaapila et al.[41] investigated the microstructure of these blends. However, there are numerous ambiguities arising from these previous studies. In particular, green emission, in the form of a so-called "g-band" PL component,[42] was observed for both undrawn and/or drawn[32,40,41] blend films. While the precise origin of the g-band remains the subject of debate,[42–45] its presence is uniformly agreed to signal the oxidation of 9,9-dialkylfluorene to 9-fluorenone moieties, a process that can affect both the PL spectral characteristics and degree of polarization. The effect of phase-separation between the polyfluorene and PE blend components on optical anisotropy is

another issue that needs to be more fully understood. Finally, He et al.[40] reported data that show that their undrawn UHMWPE-PFO blends contain a moderate fraction of chains in the β-phase conformation, while the drawn films contain both crystalline and β-phase PFO chains.[40] Both of these chain conformations strongly influence the photoluminescent behavior of PFO due to efficient excitation transfer; however, neither their origin nor their relative effect on the optical anisotropy in drawn blend films appear to be well understood.

With this background in mind, we have undertaken a study of the photophysical properties of undrawn and oriented samples of both (i) gel-processed PFO-UHMWPE blends (as studied by He et al.[40,46]) and (ii) melt-processed blends of PFO with a linear-low-density polyethylene (LLDPE). Melt-processed blends of LLDPE with conjugated polymers have previously been shown to have a microstructure that differs substantially from that of gel-processed UHMWPE blends,[47,48] but we are not aware of any studies of the anisotropic optical properties of oriented LLDPE blends with PFO. In this article, we investigate the evolution of PFO microstructure and chain conformation following tensile drawing in the two different PE hosts and the corresponding effect on the optical anisotropy and PL depolarization. We also examine the ways in which processing parameters such as drawing temperature, drawing method and PFO concentration in the blend need to be optimized for maximal optical anisotropy of the drawn blend films.

EXPERIMENTAL

Materials

PFO was supplied by the Sumitomo Chemical Company Ltd and used as received. Synthesized by the Suzuki route, it was subjected to careful purification prior to shipment. Polystyrene-equivalent gel permeation chromatography measurements yielded a weight-average molecular weight $M_w = 2.49 \times 10^5$ g/mol and polydispersity index = 2.5. As a consequence of the chain stiffness of PFO, the absolute molecular weight is a factor of $\sim$2.7 lower than the polystyrene equivalent value,[15] yielding an estimate of $\sim$190 repeat units in an average PFO chain for this polymer batch. Ultra-high molecular weight polyethylene (UHMWPE; Stamylan™ 610, $M_w = 8.7 \times 10^6$ g/mol) and LLDPE (Dowlex™ NG5056G, $\rho = 0.921$ g/cm^3, commercial pellets containing a minor fraction of the standard antioxidant) were obtained from DSM and the Dow Chemical Company, respectively, and used as received. Decahydronaphthalene (decalin; reagent grade, mixture of *cis*- and *trans* isomers) was purchased from Sigma-Aldrich, and used as received.

Fabrication of Blend Films

UHMWPE-PFO blends were "gel-processed"[37–39] by quenching semi-dilute solutions of both polymers in decalin. A 1 wt % total solute to solvent weight fraction was targeted. Approximately 5 g of UHMWPE were added to 450 g of decalin in a round-bottomed flask along with 1 wt % (based on the UHMWPE content) of Irganox 1010 antioxidant (BASF). After degassing, the mixture was placed in an oil bath at 135 °C and stirred under nitrogen until a clear solution formed. It was then left to equilibrate for a further 45 min. The required amount of PFO was dissolved in 50 g of decalin; the flask was placed into the same oil-bath to aid dissolution. The two solutions were next combined and stirred for a further 10 min under nitrogen. The PFO dispersed homogeneously in the mixture as readily demonstrated by illumination with a UV lamp, yielding spatially homogeneous PL. The mixed solution was then poured into a mold and allowed to cool, thereby forming a gel. Finally, after drying for several days under ambient conditions, blend films of $\sim$250 μm thickness were obtained.

To prepare the LLDPE-PFO blends, the required amounts of LLDPE and PFO were fed into a recycling co-rotating twin-screw mini-extruder (Eindhoven University of Technology, The Netherlands) in which they were melt-mixed at 210 °C for 10 min under nitrogen prior to extrusion. The solidified extrudate was placed between two aluminum plates and compression-molded in a hot press: initially at 230 °C for 10 min to melt the polymer blend and subsequently at 5 °C to consolidate the films. The resulting blend films were $\sim$250 μm thickness.

Tensile-drawing was carried out using an Instron model 5864 tensile tester equipped with a temperature-programmable chamber. A constant elongation rate, determined by the cross-head speed, was used for all experiments. Drawing by the hot-pin method was carried out in air over a Kofler bench preheated to 130 °C.

Fabrication of Reference Thin Films

Reference glassy PFO films were spin coated on fused silica substrates from toluene solution (10 mg/mL) at 2000 rpm to yield $\sim$100 nm thick films. Both solution and substrates were placed on a hot-plate at 100 °C for 2 min immediately prior to spin-coating in order to fully avoid the formation of β-phase in the films. Reference films containing a fraction of β-phase chain segments were prepared by exposing glassy films to saturated toluene vapour at 45 °C for 2 h. As is evident from Figure 2(c), the relative fraction of β-phase segments induced by this method is somewhat lower than in previous reports, likely due to the higher molecular weight polymer used in this study.[9,10] Reference crystalline PFO films were prepared by cooling PFO films at 5 °C/min from the nematic melt at 230 °C under nitrogen atmosphere.

Characterization

All measurements were carried out at room temperature in ambient atmosphere. Absorption spectra were measured with a dual beam Shimadzu UV-2550 spectrophotometer. An ultra-broadband wire-grid polarizer (NT68–750, Edmund Optics) was used for polarization measurements. Samples were clamped between two fused silica slides in order to reduce light scattering losses due to film corrugations. The polarizer was kept in a fixed alignment while the samples were rotated to measure absorption spectra parallel/

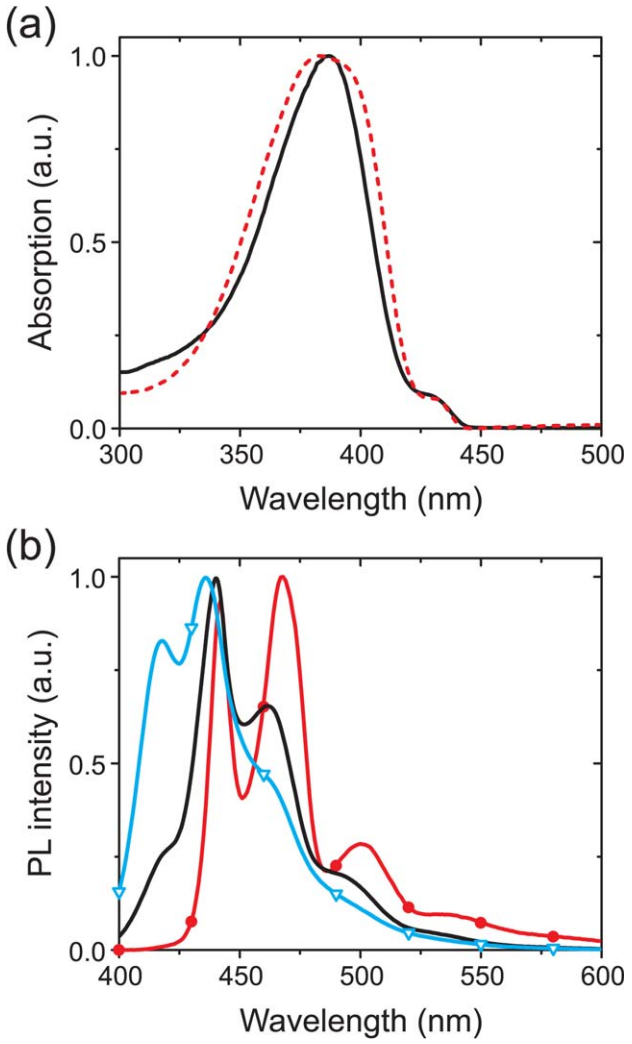

FIGURE 2 (a) Peak-normalized absorption spectra of an unoriented PFO-UHMWPE blend film containing 0.1 wt % PFO (solid black line) and a spin-coated PFO thin film containing ~3% β-phase chain segments (dashed red line). (b) Peak-normalized PL spectra of unoriented PFO-UHMWPE films containing 1 (red line + filled circles), 0.1 (black line), and 0.01 wt % (blue line-+ open triangles) PFO.

perpendicular to the orientation axis. A baseline correction file was generated for the polarizer and the two fused silica slides by recording their absorption spectrum. The absorption spectra of the drawn blend films were further corrected by subtracting the spectra measured for the corresponding neat polyethylene films of similar draw ratio and thickness. PL spectra were recorded in reflection geometry using a Jobin Yvon Horiba Fluoromax-3 spectrofluorimeter (excitation wavelength $\lambda_{ex} = 390$ nm unless stated otherwise). Films were mounted flat on a washer and wire-grid polarizers (as above) were placed before and after the sample, with the incident excitation polarization aligned parallel to the film orientation axis and the PL emission polarizer rotated about the beam axis to measure PL spectra polarized parallel/ perpendicular to the orientation axis. The perpendicularly polarized PL spectra were multiplied by the G_1 factor,[49] which corrects them for the polarization preference of the detection system. The G_1 factor was determined here for the 390–650 nm wavelength range using polarized PL measurements on dilute Coumarin 440 and Coumarin 500 laser dye solutions in ethanol, both of which are expected to be isotropic emitters. Raman spectroscopy measurements were performed using a Renishaw inVia Raman microscope in back-scattering configuration. The response of the system was calibrated using the 520 cm^{-1} peak of silicon. Linearly polarized emission from a HeNe laser at 633 nm was used as the excitation; its polarization direction was rotated by a $\lambda/2$-plate to measure Raman spectra parallel/perpendicular to the orientation axis. Detection of the scattered light was not polarized. Excitation light was focused with a 50× objective; exposure time was 3 s. No detectable photodegradation of samples occurred under these conditions. Following acquisition, the spectra were corrected by subtracting a flat dark-count background and further corrected for the polarization response of the spectrometer. The latter correction was obtained from performing the same polarized measurements on an in-plane-isotropic spin-coated PFO thin film. Wide-angle X-ray diffraction (WAXD) was performed on an Oxford Instruments Xcalibur PX diffractometer with Mo-Kα radiation (0.71 Å wavelength). For scanning electron microscopy (SEM) the films were sputter-coated with a thin layer of platinum and imaged using a JEOL JSM-6010LA microscope.

RESULTS AND DISCUSSION

Optical Spectroscopy of PFO-UHMWPE Blend Films

Unoriented Films

Blend films of PFO-UHMWPE were gel-processed from decalin solutions as described in the Experimental section. Figure 2 presents the optical spectroscopy results for undrawn PFO-UHMWPE blend films; Figure 2(a) shows the UV–vis absorption spectrum (centered on the S_0-S_1 HOMO-LUMO transition of PFO) for an undrawn blend film containing 0.1 wt % PFO. Comparison with the absorption spectrum of a 100 nm thickness spin-coated and solvent vapor annealed PFO film reveals a narrower HOMO-LUMO peak for the blend sample. The linewidth is expected to depend principally on the degree of inhomogeneous broadening, with the difference plausibly attributed to a reduced broadening for the blend film as a consequence of its long (~5 day) drying time. Slow solvent loss may assist molecular relaxation, limiting the scope for kinetically trapped nonequilibrium chain geometries that can easily occur in spin-coated films due to very rapid solvent evaporation. It is also evident, just as for the reference thin film, that the PFO-UHMWPE blend samples contain a small fraction of β-phase chain segments, yielding a characteristic β-phase peak, which appears here at 432 nm.

Figure 2(b) shows PL emission spectra of UHMWPE-based blends with PFO concentrations of 0.01–1 wt %. For the samples comprising 1 wt % PFO, the PL spectrum

corresponds closely to that for β-phase-rich spin-coated films[4,9] but with a reduced magnitude and apparent sharpening of the shortest wavelength S_1-S_0 0-0 vibronic peak due to strong self-absorption. It is known that adoption of the β-phase chain conformation can be enhanced in slow-drying films spin-coated from high boiling point solvents such as cyclopentanone[50] or in the presence of high boiling point additives such as diiodooctane.[51] Hence, the appearance of β-phase chains in PFO-UHMWPE blends cast from decalin solutions and dried over several days is expected. As the PFO concentration in the blend reduces, the dominance of the β-phase PL component decreases. This is despite there still being clear evidence of a β-phase absorption peak [see Fig. 2(a)], under which circumstances for spin-coated films the β-phase PL component normally still dominates.[51,52] This suggests that dilution of PFO in the blend may hinder the normal, highly efficient, excitation energy transfer to β-phase chains. It is also noted that the vibronic peaks in the PL spectrum for the most dilute sample with 0.01 wt % PFO are comparable to those of PFO solutions prepared with standard solvents.[53] The variations in local dielectric environment are expected to play a role in this. Heterogeneity in the dispersion of PFO within the matrix polymer may also be in part responsible for the increase in inhomogeneous broadening that limits the PL vibronic peak resolution for the 0.01 wt % PFO samples.

We also note that, contrary to previous reports for polyfluorenes in gel-processed blends with UHMWPE,[32,40,41] we do *not* observe any g-band PL emission for any of the PFO-UHMWPE blend films. The presence of 1 wt % (based on the UHMWPE content) Irganox 1010 antioxidant in our samples may be the key factor here; its use was not reported in previous studies. Use of the antioxidant did not lead to any observable changes in the absorption and PL spectra of PFO in the blends. We cannot, however, extrapolate with complete confidence that this implies that no oxidation of 9,9-dialkylfluorene to 9-fluorenone moieties occurred during processing; g-band emission can also be avoided in blend films if any oxidized segments are sufficiently dispersed to prevent excimer formation.[20]

Oriented Films

Oriented PFO-UHMWPE blend films were prepared through tensile deformation at a constant elongation rate as described in the Experimental section. Most of the data presented below is for 1 wt % PFO-UHMWPE blend films (where 1 wt % refers to the weight fraction of PFO in the blend) because this relatively high PFO concentration allows for the broadest range of characterization measurements to be conducted. A detailed investigation of more dilute ($\leq$0.1 wt % PFO) blend films is presented in section "Crystallization of PFO during Tensile Drawing."

To better understand the influence of drawing temperature, T, we studied 1 wt % PFO-UHMWPE blend films oriented in two different temperature regimes: (i) $T > 120$ °C, corresponding to the optimum[37–39] drawing temperature regime for UHMWPE and (ii) at a lower temperature, $T = 65$–68 °C, chosen to be *above* the bulk PFO glass transition temperature $T_g^{PFO} = 62$ °C but *below* the onset melting temperature of the β-phase, $T_m^{\beta} = 80$ °C.[13] Hereafter for simplicity, films drawn at temperatures above/below T_m^{β} will be referred to as hot-/cold-drawn, respectively.

Figure 3 shows the evolution of absorption spectra for hot- and cold-drawn PFO-UHMWPE films with increasing draw ratio Λ, where Λ represents the ratio of sample lengths after and before drawing. For both hot- and cold-drawn films there is a spectral distinction between parallel- and perpendicular-polarized absorption; the perpendicular spectra more closely resemble the spectrum of a blend film before drawing whilst the parallel-polarized spectra are red-shifted, consistent with uniaxial alignment of PFO chains allowing greater electronic delocalization along the chain axis. The overall optical dichroism (ratio between parallel and perpendicular absorption) increases with draw ratio from 1 (undrawn films) to $\sim$12 and 8 for $\Lambda = 100$ hot- and cold-drawn films, respectively.

For hot-drawing [see Fig. 3(a), top panel] the intensity of the characteristic β-phase absorption peak seen for undrawn blend films (see Fig. 2) reduces rapidly with draw ratio due to the drawing temperature exceeding T_m^{β}. This is consistent with previous reports on oriented PFO-UHMWPE blends where drawing temperatures $T = 90 - 100$ °C were used,[40,48] corresponding to hot-drawing conditions, which explains the observed loss of β-phase chain segments during drawing.[40] Close inspection of the spectra reveals the appearance of a poorly resolved absorption shoulder centered at $\sim$430 nm, most clearly visible in parallel-polarized spectra, which we attribute to absorption by PFO chains crystallized during the drawing process. The origin and relative orientation of these crystalline PFO chains is explored in detail in section "PFO Dispersion and Microstructure in the Blends."

As can be deduced from the spectra in Figure 3(a), lower panel, cold-drawn films retain a fraction of β-phase chains, as evidenced by the peak centered at $\sim$438 nm in both parallel- and perpendicular-polarized spectra, due to the drawing taking place at temperatures below the bulk melting temperature of the β-phase. However, despite this fact, the relative intensity of the β-phase absorption peak is found to gradually reduce with draw ratio. For example, the inset in the lower panel of Figure 3(a) shows that for the perpendicular polarized spectra the ratio of absorption intensities recorded at 438 nm (predominantly β-phase) and 360 nm (predominantly glassy), which approximately quantifies the fraction of β-phase chain segments in the sample, decreases with Λ. This indicates that, along with elevated drawing temperatures, chain motion also contributes to removing the β-phase conformation.

At this point, it is worth closely examining the nature of the glassy and β-phase conformations to understand their relative susceptibility to orientation by tensile drawing in a

UHMWPE matrix. It is interesting to note that the relative fraction of the β-phase, that is, the intensity ratio of β-phase and bulk PFO absorption peaks, is always higher for the perpendicular-polarized absorption spectra of drawn blend films—an observation that is supported by the corresponding PL data (see Fig. 4). For example, the β-phase peak is lost from the parallel-polarized spectrum for hot-drawing even at a relatively low draw ratio of 10, at which the peak is still clearly visible in the perpendicular-polarized spectrum. We advance the following explanation [see Fig. 3(b)]:

1. Tensile drawing forces the wormlike glassy PFO chains to orient along the drawing axis; thus the apparent intensity of the bulk PFO absorption increases/decreases for parallel-/perpendicular-polarized excitation, respectively.
2. The β-phase chain segment conformation of PFO is characterized by a unique inter-monomer torsion angle[2,11] (see Fig. 1) that would make a β-phase segment analogous to a 1D crystal embedded in a disordered matrix. Hence, it becomes clear that *the existing metastable β-phase chain segments cannot be easily aligned* because any adverse physical motion of the chain might disrupt the well-defined conformation of the β-phase segment, converting it into a wormlike glassy segment. The removal of β-phase by chain motion would occur isotropically, that is, irrespective of the relative chain orientation, and thus the magnitude of the β-phase absorption peak decreases equally for both parallel- and perpendicular polarized spectra. We note that this explanation is fully consistent with previous reports on oriented β-phase PFO thin films, in which β-phase was invariably introduced by postprocessing.[15,22,26]

The combined result is a higher relative fraction of β-phase in the perpendicular-polarized spectra. For additional details and spectroscopic evidence, see Figure S1, Supporting Information.

Figure 4 presents the PL spectra for 1 wt % PFO-UHMWPE blend films hot- and cold-drawn to $\Lambda = 70$, obtained under parallel-polarized excitation (incident E-vector oriented along the drawing axis) and for both parallel- and perpendicular-polarized detection. Both of the hot-drawn blend film PL spectra (with vibronic peaks at 433, 457, and 488 nm in the parallel- and at 436, 457, and 487 nm in the perpendicular-polarized detection data) are a superposition of the glassy PFO PL spectrum (with vibronic peaks at 421, 447, and 476 nm as measured for a reference spin-coated glassy film) and the PL of crystalline PFO. The spectroscopic signature of crystalline PFO in hot-drawn blend films was already observed as a shoulder at ~430 nm in the corresponding absorption spectra [see Fig. 3(a), top panel]. PL spectrum of

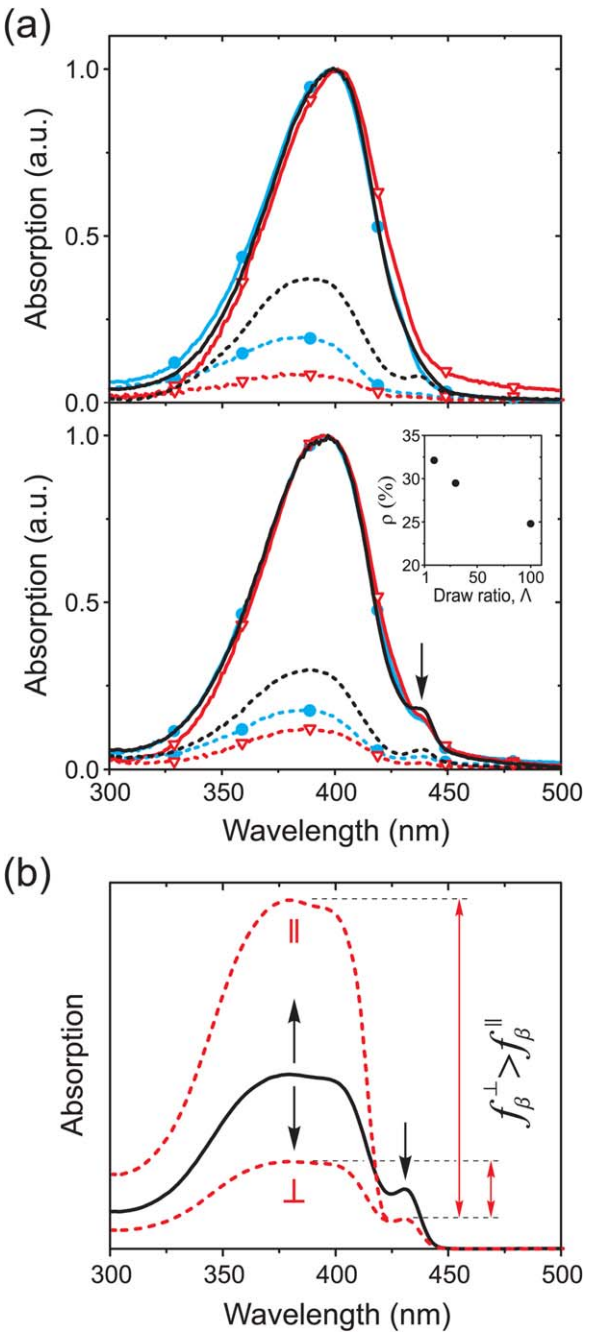

FIGURE 3 (a) Absorption spectra of (top panel) hot- and (bottom panel) cold-drawn 1 wt % PFO-UHMWPE blend films, recorded with the incident light polarized parallel (solid lines) and perpendicular (dashed lines) to the drawing axis and normalized by the peak absorption of the respective parallel-polarized spectra. Data are shown for films with draw ratios $\Lambda = 10$ (black lines), 30 (blue lines + filled circles), and 100 (red lines + open triangles). The arrow in the lower panel indicates the position of the β-phase absorption peak (438 nm). The inset in the lower panel shows the percentage ratio, ρ, of absorption intensities measured for the perpendicular-polarized spectra at 438 (β-phase) and 360 nm (predominantly glassy). (b) Schematic illustration of the effect of drawing on the absorption and relative fraction of the β-phase chains, f_β, of PFO in undrawn (solid black line) and drawn (dashed red lines, polarizations indicated) blends with UHMWPE. Arrows indicate the direction of changes to the spectrum at the main PFO π-π^* HOMO-LUMO peak and at the long wavelength β-phase peak.

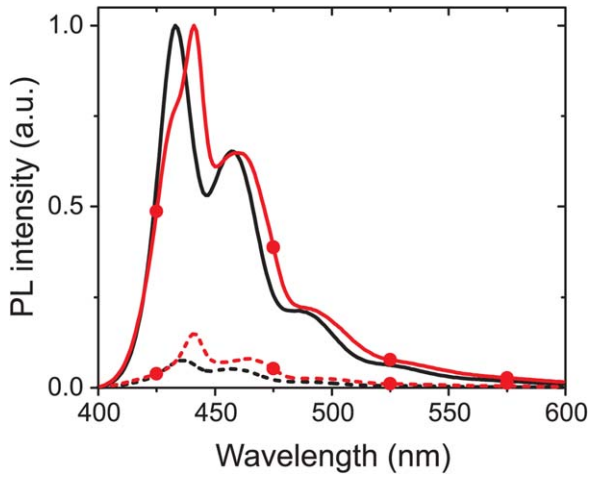

FIGURE 4 Polarized PL spectra of 1 wt % PFO-UHMWPE blend films hot- (black lines) and cold-drawn (red lines + filled circles) to draw ratio $\Lambda = 70$ showing emission polarized parallel (solid lines, peak normalized) and perpendicular (dashed lines) to the drawing axis.

crystalline PFO chains in hot-drawn blend films is obtained by direct photoexcitation at this absorption shoulder and features a well-defined vibronic progression with peaks at 435, 461, and 492 nm (see Fig. S2, Supporting Information).

The PL spectrum of the cold-drawn blend film comprises a superposition of the typical β-phase PL spectrum (with vibronic peaks at 440, 465, and 500 nm[9]) and that of the hot-drawn blend film. This observation is consistent with the retention of a β-phase absorption peak at high draw ratios, as shown in Figure 3(a) (lower panel). The fact that the β-phase PL does not totally dominate the PL spectrum here indicates that excitation energy transfer is more limited in the blend than it would be in a PFO thin film with a similar fraction of β-phase chain segments. Whether this is a signature of heterogeneity, or a change in excitation dynamics remains to be resolved. We also note that the β-phase PL contribution is stronger for the perpendicular-polarized PL spectrum which is consistent with the higher relative fraction of the β-phase for chain orientation perpendicular to the drawing axis (see Fig. S1, Supporting Information). We further note that parallel-polarized excitation tends to downplay this effect.

The deduced variation in emission anisotropy is presented in Figure 5 as a function of draw ratio for both hot- and cold-drawn 1 wt % PFO-UHMWPE blend films. To allow direct comparison with the data of He et al.[40] we have used a simplified PL emission anisotropy ratio, R, calculated as the ratio of integrated intensities for the PL spectra polarized parallel and perpendicular to the drawing axis, in both cases under parallel-polarized excitation.[54] In essence, R quantifies the degree of PL emission depolarization following parallel-polarized excitation.

We observe from Figure 5 that for hot-drawn films R increases up to $\Lambda = 70$ and then begins to saturate. For cold-drawn films, the increase in R is linear up to the highest draw ratios with no apparent saturation, albeit that the increase with draw ratio has a shallower slope. The cold-drawn films, for which the PL spectra have a substantial β-phase emission component, show markedly lower R values than hot-drawn blend films for which there is no β-phase emission. This latter situation, at first sight, appears to be at odds with the previously demonstrated higher natural emission anisotropy of the β-phase conformation associated with its more axial transition dipole moment.[15] The reasons for this are related to the inability of the existing β-phase chain segments to be oriented by tensile drawing (as discussed above and in section "PFO Dispersion and Microstructure in the Blends" below), which in turn means that their presence in drawn films contributes strongly to PL emission depolarization thereby leading to a reduction of the corresponding R value.

At this point, we conclude the description of the evolution of microstructure and PL anisotropy with draw ratio for PFO-UHMWPE blend films. Given the complexity of the observed behavior, we sought to explore in greater detail the microstructure of the drawn blends as well as the other factors that limit the optical anisotropy of these blends. Section "Factors Influencing Optical Anisotropy and Photoluminescence Depolarization in Drawn PFO-UHMWPE Blend films" considers the role of drawing temperature and method on optical anisotropy and explores the relationship between the blend film microstructure, PFO crystallization, and PL emission depolarization.

Factors Influencing Optical Anisotropy and PL Depolarization in Drawn PFO-UHMWPE Blend Films

Drawing Mechanics: Tensile Tester versus Hot-pin Methods

The absence of branching in UHMWPE implies that orientation of the guest PFO polymer during tensile drawing proceeds primarily through shear forces and, possibly, epitaxial

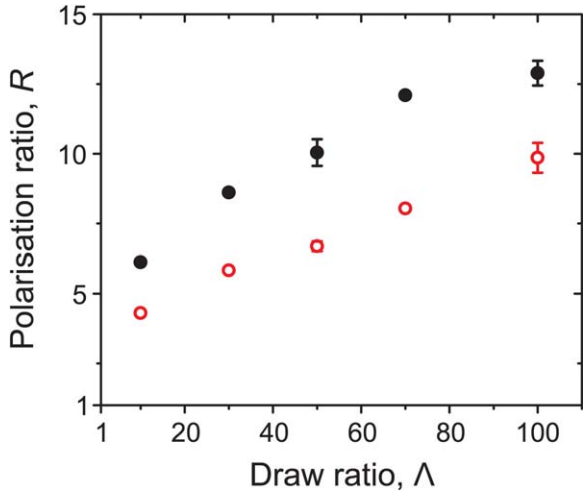

FIGURE 5 PL emission anisotropy ratio, R, for hot- (filled black circles) and cold-drawn (open red circles), 1 wt % PFO-UHMWPE blend films as a function of draw ratio, Λ. Representative error bars are shown for films with draw ratios $\Lambda = 50$ and 100.

TABLE 1 Comparison of the Influence of Drawing Methods on the PL Emission and Raman Scattering Anisotropies of 1 wt % PFO-UHMWPE Blend Films

Method	Temperature (°C)	Draw Ratio Λ	PL Anisotropy Ratio R	Raman Anisotropy	
				1605 (cm^{-1})	1130 (cm^{-1})
Tensile Tester	130	50	10.0	13.3	8.7
Hot-Pin	130	40	14.4	15.9	8.0

phenomena. With respect to shear forces, alignment of the guest within the UHMWPE matrix is expected to depend on the drawing mechanics. In this section, we present a brief comparison between two of the main uniaxial tensile drawing techniques.

In previous studies on oriented UHMWPE-polyfluorene blends,[32,40,41] drawing of films was carried out by a "hot-pin" method. This typically involves manual stretching of the films over a heated plate or bar, such as a Kofler bench, held at the required temperature. In our study, however, we used a tensile tester fitted with a temperature programmable chamber. The subtle, yet important, difference between these two methods is readily understood in terms of the relationship between rate of elongation and incremental strain rate, with the latter defined as

$$\frac{d\varepsilon}{dt}=\frac{d}{dt}\left(\frac{l_2-l_1}{l_1}\right)=\frac{d}{dt}\left(\frac{\Delta l}{l_1}\right) \quad (1)$$

where l_2 and l_1 are the sample lengths following and prior to incremental drawing, ε is the incremental strain and Δl is the incremental elongation.

In the case of "hot-pin" drawing, l_1 is defined by the length of sample contact with the hot plate and thus remains constant. Assuming also an approximately constant rate of elongation, it can be seen from (1) that the strain rate, and hence the orienting stress applied to the guest polymer, *does not vary* with draw ratio.

However, for drawing with a tensile tester using a constant elongation rate (i.e., constant Δl per unit time), it can be seen from (1) that the strain rate *decreases* with increasing sample length. A reduced strain rate at high draw ratios is expected to decrease the efficiency of guest orientation by making chain recoil/relaxation more favorable. This fact may contribute to the observed saturation of PL anisotropy at high draw ratios for the 1 wt % PFO-UHMWPE blend films hot-drawn with the tensile tester (see Fig. 5).

We confirmed the influence of drawing method through a direct comparison of samples oriented by tensile tester and "hot-pin" drawing techniques. Table 1 reports the results for two samples cut from a single undrawn blend film and then hot-drawn (at 130 °C) (i) using the tensile tester and (ii) over a Kofler bench (hot-pin). Whilst the final draw ratios, 50 and 40, respectively for the tensile tester and Kofler bench, were of a similar magnitude, a constant strain rate was maintained for the hot-pin drawing. Drawing by the hot-pin method led to a significant improvement in PFO orientation, as evidenced by a 1.4-fold increase in emission anisotropy relative to the $\Lambda = 50$ tensile-tester drawn sample. Polarized Raman measurements (see section "Drawing Temperature: Hot- versus Cold-Drawing" below) showed a similar 1.2-fold increase in the 1605 cm^{-1} PFO aromatic ring stretching mode anisotropy. We note that this improvement in PFO orientation for the $\Lambda = 40$ hot-pin drawn film has been achieved despite the somewhat lower Raman anisotropy of the 1130 cm^{-1} PE symmetric C—C stretching mode, which confirms that the lower draw ratio of this film relative to that of the tensile-tester drawn sample corresponds to a lower uniaxial order parameter.

Drawing Temperature: Hot- versus Cold-Drawing

Temperature is known to strongly affect the drawability of polyethylenes. Studies on melt-crystallized linear polyethylene[55] showed that maximum, efficient deformation is possible only within a relatively narrow temperature window. Similarly, although gel-processed UHMWPE films could be drawn even at room temperature,[56] their drawability was found to be significantly improved for temperatures closer to the polymer melting temperature, T_m.[38] This is explained by temperature-enhanced chain mobility facilitating chain alignment under the applied tensile stress.

Raman Spectroscopy

The relative alignment of PFO and UHMWPE polymer chains in hot- and cold-drawn films was studied using polarized Raman spectroscopy, a technique that relies on (i) there being spectrally separated characteristic vibrational modes associated with specific subunits of molecular structure and (ii) these modes having vibrational displacement vectors linked to the local molecular structure and its orientation. Molecular orientation can then be probed by the spectrally resolved, polarization selective excitation and detection of Raman scattered light.[57–59] UHMWPE and PFO both have specific vibrational modes characterized by a uniaxial Raman scattering tensor, the principal axis of which is closely aligned with the polymer backbone. In the case of PFO it is the 1605 cm^{-1} C—C ring-stretching mode that we use,[57,58] whereas for UHMWPE, it is the symmetric C—C stretching mode at 1130 cm^{-1}.[59]

Figure 6 presents Raman anisotropy data as a function of draw ratio for the 1130 and 1605 cm^{-1} vibrational modes

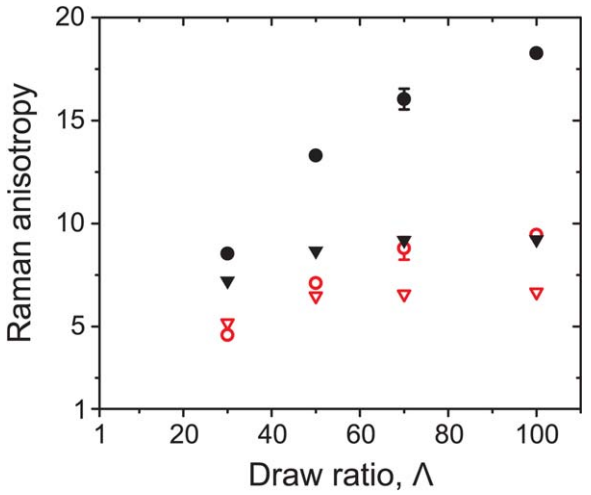

FIGURE 6 Draw ratio dependence of the anisotropy of PFO 1605 cm^{-1} (circles) and UHMWPE 1130 cm^{-1} (triangles) Raman modes measured for hot- (filled black symbols) and cold-drawn (open red symbols) 1 wt % PFO-UHMWPE blend films. Representative error bars are shown for films with draw ratio $\Lambda = 70$.

measured for 1 wt % PFO-UHMWPE blend films following hot- and cold-drawing. Raman anisotropies were calculated as the ratio of maximum intensities for Voigt fits to the two Raman peaks measured with incident light polarized parallel and perpendicular to the drawing axis. Representative spectral data is included in Figure S3 of the Supporting Information.

It is clear from Figure 6 that uniaxial alignment of UHMWPE chains proceeds far less efficiently in the 65–68 °C cold-drawing regime than in the 125–140 °C hot-drawing regime. Alignment of the matrix will strongly affect alignment of the PFO guest and it is then no surprise that PFO chains are less well aligned for the cold-drawn samples. The fact that the anisotropy of the 1130 cm^{-1} mode is lower than that of the 1605 cm^{-1} mode for both hot- and cold-drawing is consistent with the 1130 cm^{-1} mode not being fully aligned along the polyethylene chain axis.[59]

We also note that the 1605 cm^{-1} Raman mode anisotropy for both hot- and cold-drawn films appears to saturate beyond $\Lambda = 70$. This is different to the corresponding PL emission anisotropy data (see Fig. 5) where we see a similar saturation of R for hot-drawn films but *not* for cold-drawn films, for which R increases with draw ratio over the entire range. This discrepancy in the emission and Raman anisotropy data for the cold-drawn films is explained by the fundamental difference between the two measurements: Raman anisotropy measurements probe the molecular orientation of the entire ensemble of chains in the sample, while emission originates from a subset of chains within the low energy tail of the density of states, following excitation energy transfer from the ensemble. Energetically low lying sites are expected to be those with more extended conjugation[60] and/or those situated within a more polarizable local environment. As will be shown in section "PFO Dispersion and Microstructure in the Blends", the degree of orientation of the minority low-energy crystalline and β-phase chain segments can be substantially different to that of the bulk glassy chain ensemble.

The combined PL emission and Raman anisotropy measurements show that macroscopic chain orientation is not the only factor determining the optical anisotropy of the drawn blend films and indicate that PFO microstructure in the blends is likely to be of key importance. Due to this complexity of behavior and morphological heterogeneity of the system we refrain from presenting the usual macroscopic chain order parameter calculations[57,58] which, in this case, would be expected to be inexact and misleading.

X-Ray Diffraction and SEM

WAXD and SEM results, summarized in Figure 7, provide further insight into the differences in microstructure for PFO-UHMWPE blends drawn in the two temperature regimes. The equatorial WAXD data for the blend films [see Fig. 7(a,d)] shows that in hot-drawn films UHMWPE very rapidly adopts a double chain orientation[39,61] as evidenced by the systematic absence of the (200) and (210) peaks and a concomitant enhancement of the (020) peak intensity, even for draw ratios as low as 10.

Double orientation of UHMWPE films means that, in addition to near-perfect alignment of c-axis in the drawing direction (i.e., fiber orientation), the b- and a-axis are also well-oriented parallel and perpendicular to the film plane, respectively. Such morphological perfection is characteristic of (near) single-crystalline order and signifies a very high degree of chain alignment and order. Complete double orientation is not, however, observed for cold-drawn films even for draw ratios up to 100, which, in agreement with the Raman anisotropy results presented in Figure 6, indicates a lower degree of chain alignment. We note that, due to its low concentration in the blend, we could not observe any diffraction signal from PFO in the WAXD data for the blend films.

The SEM micrographs of $\Lambda = 100$ blend films [see Fig. 7(b,c,e,f,)] show that hot-drawn film has a smooth film surface with few defects in the highly regular fibrillar texture. The striations that appear approximately perpendicular to the drawing axis, seen most clearly in Figure 7(c), are the kink bands typically observed in highly oriented PE samples. Splicing of the film along the drawing axis is evident, resulting from near-perfect chain orientation reducing the number of tie chains. However, the cold-drawn film surface exhibits a large number of imperfections; comparison with the SEM micrograph of an undrawn blend film (see Fig. S4 in the Supporting Information) suggests that the irregularities in the texture of the cold-drawn film are the residual unoriented regions of UHMWPE. Their presence is easily understood to be the result of reduced chain mobility of PE in the cold-drawing regime preventing the complete orientation of entangled regions. As will be shown in the following section,

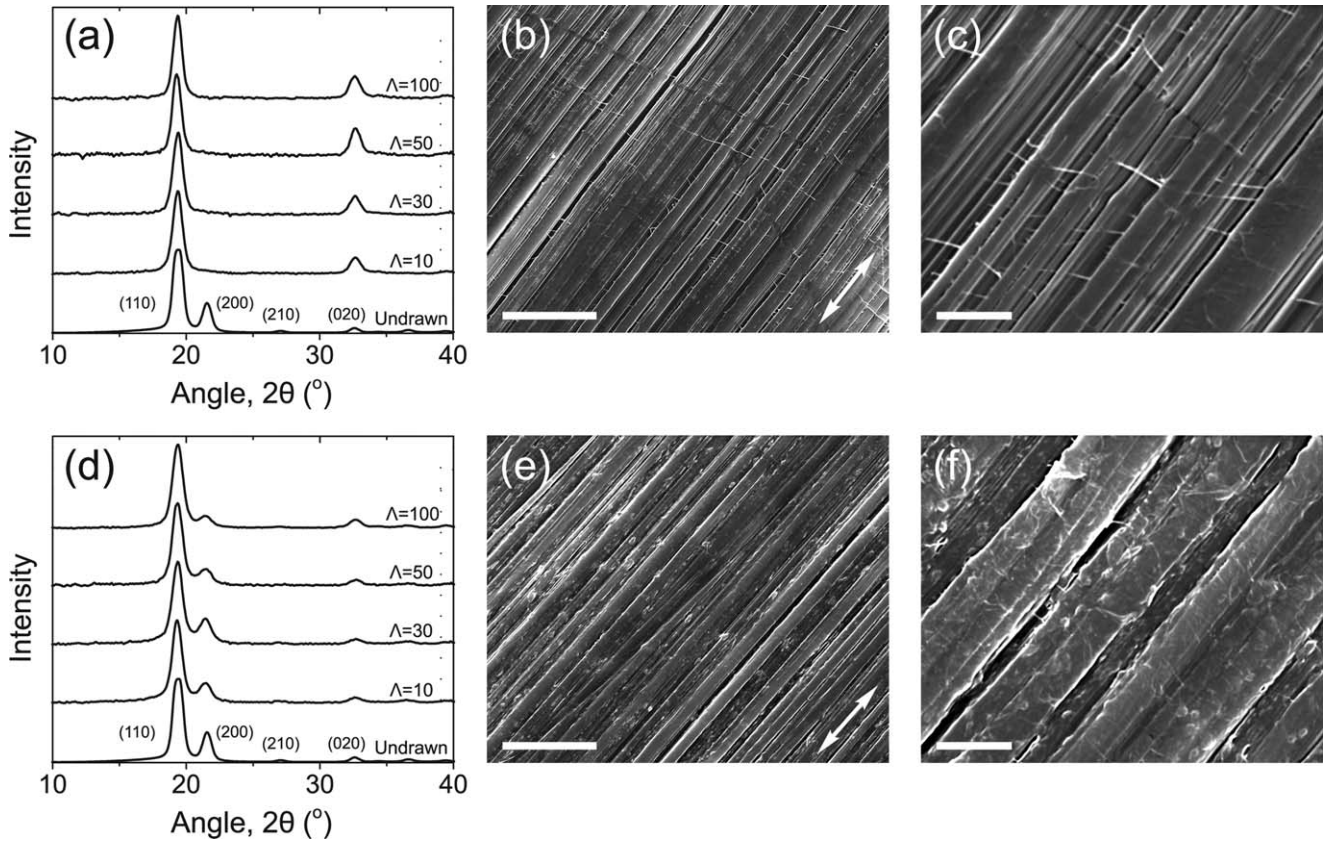

FIGURE 7 (a,d) Equatorial WAXD patterns of 1 wt % PFO-UHMWPE blend films with draw ratios Λ indicated. (b,c,e,f) Scanning electron micrographs of Λ = 100 blend films with (b, e) 50 μm and (c, f) 10 μm scale bars. The data is shown for hot- (upper panels) and cold-drawn (lower panels) films.

the distinct microstructure of PFO located within these unoriented regions leads to stronger PL depolarization for the cold-drawn films.

PFO Dispersion and Microstructure in the Blends

The degree of dispersion of a conjugated polymer guest in a PE matrix is known to strongly affect its orientation behavior during tensile drawing. Previous work by Montali et al. demonstrated that phase-separation between the guest and host obstructs the achievement of high optical anisotropy for the guest polymer.[35] These authors studied poly(2,5-dioctyloxy-1,4-diethynylphenylene-*alt*-2,5-bis(2'-ethylhexyloxy)-1,4-phenylene) (EHO-OPPE) in gel-processed blends with UHMWPE and found that efficient alignment of the EHO-OPPE chains along the drawing direction occurs only following dispersal of any phase-separated clusters existing within the undrawn film. This is expected to apply equally to PFO-UHMWPE blends. Another consideration for PFO is the presence of lower HOMO-LUMO transition energy crystalline and/or β-phase conformations which, following efficient excitation transfer from the bulk glassy chains, dominate the PL emission properties of blend films.

Polarized PL excitation (PLE) spectroscopy provides a versatile technique for observing the changes in PL emission anisotropy as a function of excitation wavelength and, hence, the different conformational and microstructural subsets of polymer chains that are excited at different wavelengths. In a typical measurement, the excitation wavelength, λ_{ex}, is scanned across the absorption spectrum of the sample while the PL intensity is monitored at a fixed wavelength. The polarization of the excitation light is parallel to the drawing axis, while the PL is detected with polarizations both parallel and perpendicular to the drawing axis. PLE anisotropy, calculated from the ratio of the PL intensities polarized parallel and perpendicular to the drawing axis, provides information about the relative PL depolarization across the density of states, recognizing of course that (due to the off-axis component of the optical transition dipole) parallel-polarized excitation can also excite perpendicularly oriented chains. Despite its potential, we are not aware of any polarized PLE data previously reported for oriented UHMWPE—conjugated polymer blends.

Polarized PLE spectra are presented in Figure 8 for 1 wt % PFO-UHMWPE blend films hot- and cold-drawn to draw ratio Λ = 70. The PLE spectra were measured for emission at 457 and 465 nm for hot- and cold-drawn films corresponding to their respective S_1-S_0 0-1 vibronic peaks (see Fig. 4). Typically, for a homogeneous uniaxially oriented ensemble of

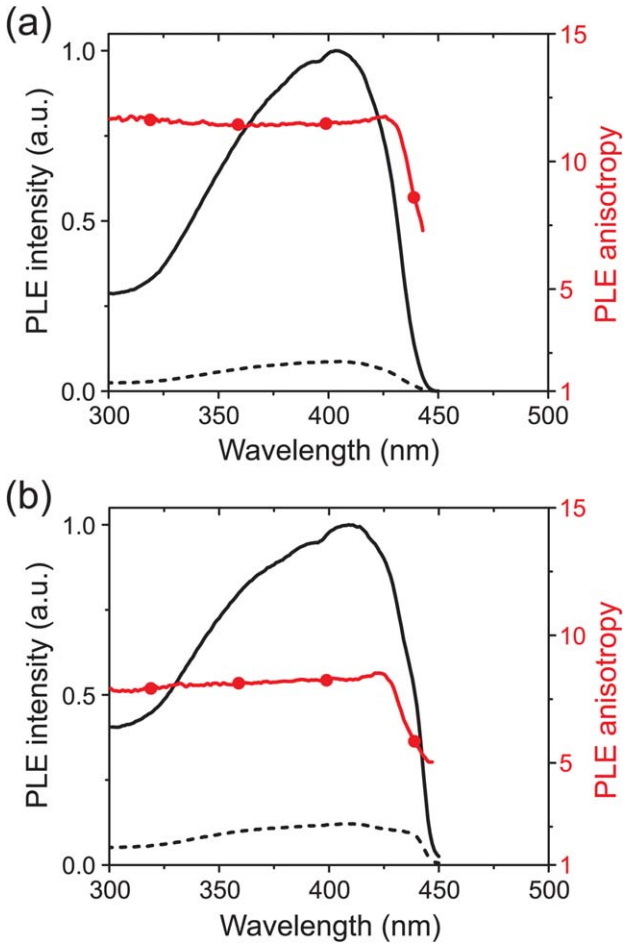

FIGURE 8 PLE spectra (black lines, left ordinate) of (a) hot- and (b) cold-drawn, $\Lambda = 70$, 1 wt % PFO-UHMWPE blend films for emission polarized parallel (solid lines) and perpendicular (dashed lines) to the drawing axis taken under parallel-polarized excitation. Also shown (red lines + filled circles, right ordinate), in each case, are the corresponding PLE anisotropy spectra.

conjugated polymer chains, excitation of the lowest energy chromophores limits depolarizing energy transfer, resulting in maximized values of PLE anisotropy at the red edge of the excitation spectrum.[62] Interestingly, we do not observe this; for both hot- and cold-drawn films (see Fig. 8), PLE anisotropy is constant over a large part of the excitation spectrum but then drops abruptly for $\lambda_{ex} \geq$ 425 nm. The position of the down-step for hot-drawn films closely matches the position of the shoulder observed for both PLE and absorption spectra [see Fig. 3(a), top panel] at ~430 nm and attributed to a fraction of PFO chains that crystallized during the drawing process. For cold-drawn films, there is a lower overall PLE anisotropy, consistent with the PL emission anisotropy data presented in Figure 5. The onset of the drop in PLE anisotropy occurs in the region of S_0-S_1 0-0 β-phase absorption [see Fig. 3(a), bottom panel], where the PLE spectra themselves also show, albeit rather indistinctly, a shoulder due to the presence of β-phase segments.

The PLE anisotropy data suggest that the crystalline and β-phase chain segments found in hot- and cold-drawn 1 wt % PFO-UHMWPE blend films are relatively poorly aligned with respect to the drawing axis. This is a concern in relation to optical anisotropy, since the normally efficient excitation energy transfer that occurs from other chain segments will, as a consequence, tend to reduce the PL anisotropy.

We propose that the poor relative alignment of crystalline and β-phase PFO chain segments in drawn 1 wt % PFO-UHMWPE blend films is a consequence of the initial phase-separated microstructure of the undrawn blend film (cf. schematic illustration in Fig. 9). Thermal analysis data shows no evidence for the miscibility of PFO and PE (see Fig. S5 in the Supporting Information for further details), which is expected due to thermodynamic incompatibility of most macromolecules.[47,48] Casting their mixture from dilute solution followed by slow evaporation of solvent results in a phase-separated microstructure for the dried blend film. As the solvent evaporates and the concentration of PFO in the cast solution exceeds the value required for chain overlap,[63] gelation of PFO will occur. This is known from the literature[15,63,64] to feature (i) the formation of physical cross-links and (ii) the adoption of the β-phase conformation by a fraction of chain segments. The microstructure of the undrawn blend films is schematically illustrated in Figure 9(a), the key element being the existence of a fraction of PFO chains in phase-separated β-phase-rich clusters.

Hot-drawing the 1 wt % PFO-UHMWPE blend films results in an efficient and homogeneous orientation of the UHMWPE matrix. However, the PFO used in this study melts with onset at 160 °C and this temperature does not change upon its incorporation into the PE matrix (see Fig. S5, Supporting Information). From previous reports on similar blends we expect that, since the drawing temperature is below T_m of bulk PFO, the dispersion of phase-separated PFO clusters during drawing would proceed solely through mechanical interaction with the orienting UHMWPE chains.[48,65] The resulting inefficient dispersal of PFO clusters, combined with the reduction of strain rate at higher draw ratios (see section "Drawing Mechanics: Tensile Tester versus Hotpin Methods"), implies that clusters of poorly oriented PFO chains can exist even in highly drawn 1 wt % PFO-UHMWPE films [cf. schematic illustration in Fig. 9(b)]. At the same time, since the drawing temperatures are greater than the bulk T_g of PFO,[2,12,14] crystallization of PFO should take place provided confinement effects are not severe.[66] Such crystallization would occur most rapidly in PFO-rich clusters. Under these circumstances, excitation energy transfer to the poorly oriented crystalline PFO chains contained within these clusters would indeed lead to PL depolarization, as demonstrated in Figure 8(a). Conversely, drawing temperatures above T_m^{β} ensure that no β-phase PFO chain segments are present in the hot-drawn blend films.

In the case of cold-drawn films, we consider that the lower mobility of UHMWPE chains at reduced temperatures ensures that a fraction of poorly-aligned regions [cf. Fig.

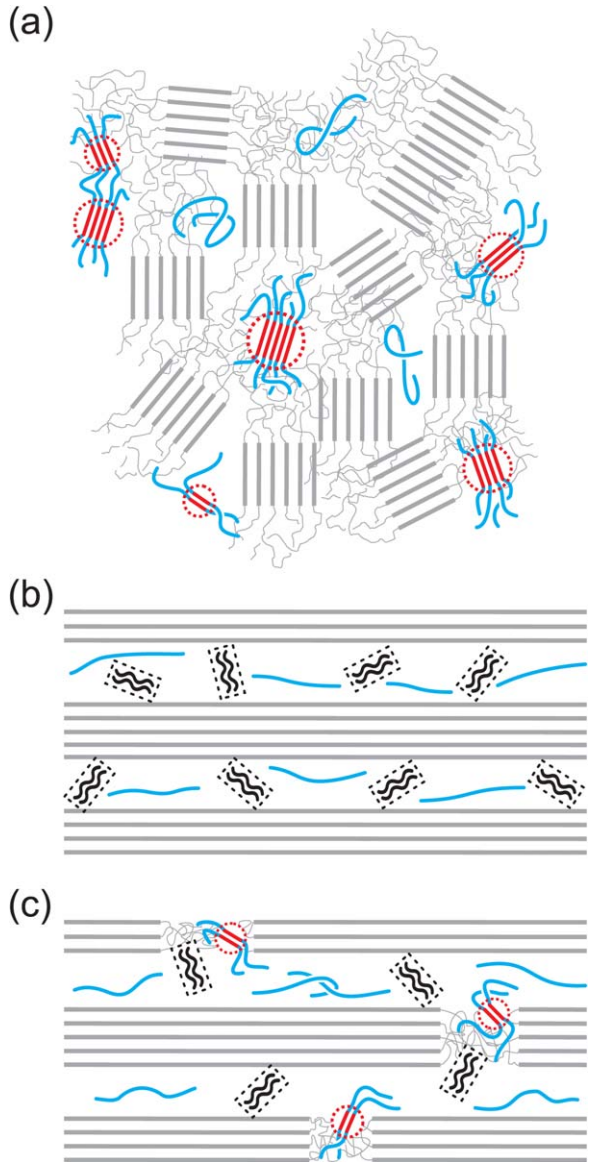

FIGURE 9 Schematic illustration of chain dispersion and microstructure in 1 wt % PFO-UHMWPE blend films: (a) undrawn, (b) hot-drawn, and (c) cold-drawn. PE and glassy PFO chains are represented by gray and blue lines, respectively. PFO clusters containing crystalline and β-phase chain segments are represented by paired black zig-zag lines and red straight lines, respectively. The relative fractions of crystalline and β-phase chain segments are exaggerated.

7(e,f)] remain, wherein there can exist phase separated PFO clusters retaining a fraction of β-phase chain segments, as is schematically illustrated in Figure 9(c). Tensile stress cannot be fully transferred to the PFO chains contained within these clusters, limiting both their dispersal within the UHMWPE host and their alignment. Moreover, since the β-phase segments have a lower-lying first electronic excited state than glassy PFO, we expect that they will be the preferred destination for rapid excitation energy transfer from, conceivably, better oriented glassy chains, thereby also contributing to the PL depolarization observed in Figure 8(b).

Crystallization of PFO During Tensile Drawing

To further study crystallization of PFO during tensile drawing, we prepared more dilute PFO-UHMWPE blends containing 0.1 and 0.01 wt % PFO, which were subsequently hot- and cold-drawn to draw ratio $\Lambda = 50$. PLE anisotropy spectra for the oriented films are shown in Figure 10. In stark contrast to the results for oriented blend films with higher PFO concentration (cf. Fig. 8), it is immediately clear that PLE anisotropy increases at the red-edge of the excitation spectrum. This suggests that (i) phase-separated PFO clusters present in the corresponding undrawn films are more readily dispersed during drawing and/or (ii) PFO clusters that remain are less readily populated by excitation energy transfer from well-aligned chains, at least to the degree that they no longer strongly influence the resulting optical properties.[48] Whereas poorly oriented PFO clusters are believed to remain even in highly drawn 1 wt % PFO-UHMWPE films, in the more dilute 0.1 wt % PFO-UHMWPE films the dispersal of PFO clusters is considered more likely due to their smaller size, proportional to the PFO concentration in the blend. We also note that, as for blend films with higher PFO concentration, the PLE anisotropy values of the drawn 0.1 wt % PFO-UHMWPE films are higher for the hot-drawing conditions due to more efficient orientation of the UHMWPE matrix.

The PL spectra (not shown) of PFO-UHMWPE blend films containing 0.1 and 0.01 wt % PFO drawn to $\Lambda = 50$ were found to be a superposition of PL spectra from two emitting species:

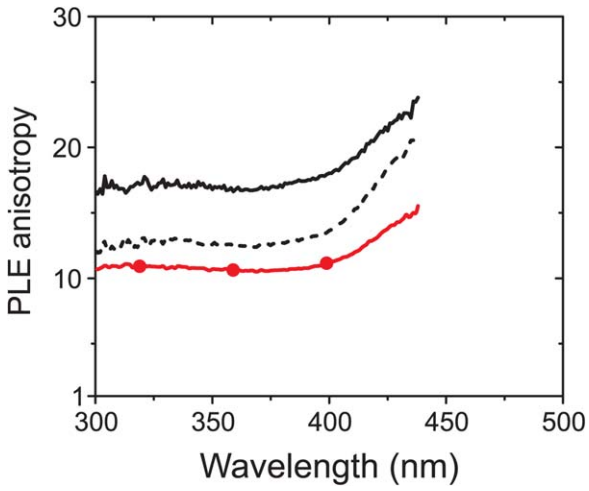

FIGURE 10 PLE anisotropy spectra of 0.1 wt % PFO-UHMWPE blend films hot- (solid black line) and cold-drawn (solid red line + filled circles) to draw ratio $\Lambda = 50$. The PLE anisotropy of an even more dilute (0.01 wt % PFO) blend film hot-drawn to draw ratio $\Lambda = 50$ is also shown for reference (dashed black line).

TABLE 2 Summary of PL Anisotropy and PL Crystalline Fraction Results for 0.1 and 0.01 wt % PFO-UHMWPE Blend Films Drawn to $\Lambda = 50$

PFO Concentration in the Blend (wt %)	Hot/Cold Drawing Regime	PL Emission Anisotropy Ratio R ($\lambda_{ex} = 390$ nm)	PL Crystalline Fraction		
			Parallel-Polarized (%)	Perpendicular-Polarized (%)	Parallel/Perpendicular Ratio
0.1	Hot	14	59	47	1.3
0.01	Hot	12	44	27	1.6
0.1	Cold	10	39	27	1.4
0.01	Cold	9	26	15	1.7

Excitation was polarized parallel to the drawing direction and deconvolution results are reported for parallel- and perpendicular-polarized emission.

1. Glassy PFO chains, as found for glassy films spin-coated from solutions in good solvents.[9]
2. Crystalline PFO chains, the PL spectrum of which is clearly revealed by direct photoexcitation at 432 nm, corresponding to the spectral position where absorption by crystalline chains is prevalent.[4,12]

We note that no β-phase PL contribution was detected for these drawn films, suggesting that β-phase-rich PFO clusters present in the undrawn blend film are dispersed, thereby turning off excitation energy transfer to β-phase chain segments and/or eliminating the β-phase conformation altogether. The latter finding is consistent with the proposal that chain motion during drawing removes the β-phase conformation. The low PFO fraction and consequently small optical density of these drawn films prevents us from using absorption spectroscopy to confirm the absence of β-phase segments.

To investigate the nature of the crystalline PFO chains and their effect on optical anisotropy, we have used a simple PL deconvolution method to determine the relative contributions of crystalline PFO to the overall PL emission spectra and correlated these results with PL emission anisotropy ratios R measured for the same films; the results are summarized in Table 2. For details of the PL deconvolution, the reader is directed to Figure S6 of the Supporting Information.

The most important observation is that the PL crystalline fraction is invariably higher in the emission spectra polarized parallel to the drawing axis, which is strong evidence for PFO *crystallization under strain*, whereby the polymer chains crystallize with their long axis preferentially oriented in the direction of the uniaxial mechanical deformation. The fact that the overall PL emission anisotropy of the drawn blend films, quantified by R, is proportional to the PL crystalline fraction in their respective parallel-polarized spectra confirms our proposal that PFO crystallizes during the drawing process, yielding the most well-oriented subset of chains.

On a cautionary note, we should mention that, since we are dealing with PL measurements, additional effects due to concentration dependent and anisotropic excitation energy transfer cannot be ruled out. For example, the data in Table 2 also appears to suggest that the relative anisotropy of the PL crystalline fraction is higher for the most dilute 0.01 wt % PFO-UHMWPE blends. This is likely to be a result of increasing chain dilution limiting the occurrence of depolarizing excitation energy transfer following *parallel*-polarized excitation, which in turn leads to underestimation of the crystalline fraction in the *perpendicular*-polarized PL spectra. For the same reason, the smaller size of crystalline PFO domains in cold-drawn relative to hot-drawn films (for a given concentration), resulting from reduced chain mobility at lower temperatures, may also be responsible for the increase in crystalline PL fraction anisotropy due to more limited depolarizing excitation energy transfer within the smaller crystallites. Despite these nuances, we consider that it remains highly plausible that PFO crystallization occurs under strain in these blends; our interpretation of polarized PL and PLE data here is further supported by absorption dichroism measurements performed on oriented PFO-LLDPE films in section "Optical Spectroscopy of PFO-LLDPE Blend Films."

Finally, we wish to outline the basic thermodynamics of PFO crystallization during drawing in UHMWPE-based blends and the implications thereof. The mechanical stretching of worm-like glassy PFO chains "dissolved" in UHMWPE strongly reduces their conformational entropy, thus also reducing the entropic penalty of crystallization. At the same time, the chemical similarity between PE and the alkyl side-chains of PFO implies that well-oriented UHMWPE fibers can provide a nucleation surface for *side-chain-driven epitaxial crystallization* of PFO. Epitaxial crystallization of PFO has already been observed in friction-transferred oriented films following thermal annealing.[23] In this case, such crystallization would be influenced by the usual parameters, including concentration and temperature. As shown by the results in Table 2, for a given concentration the crystalline PL fraction was lower for the cold-drawn samples, likely due to the reduced chain mobility hindering efficient crystal growth. Crystallization of PFO during drawing in PFO-UHMWPE blends and its effect on the resulting optical properties certainly deserve further exploration. For example, it is very likely that, due to stronger interchain bonding within the crystal, crystallization of PFO during drawing can prevent chain relaxation and thus allow optimal alignment to occur. Such a situation also occurs in the drawing of precursor-route poly(*p*-phenylenevinylene)—further complicated by plasticization with

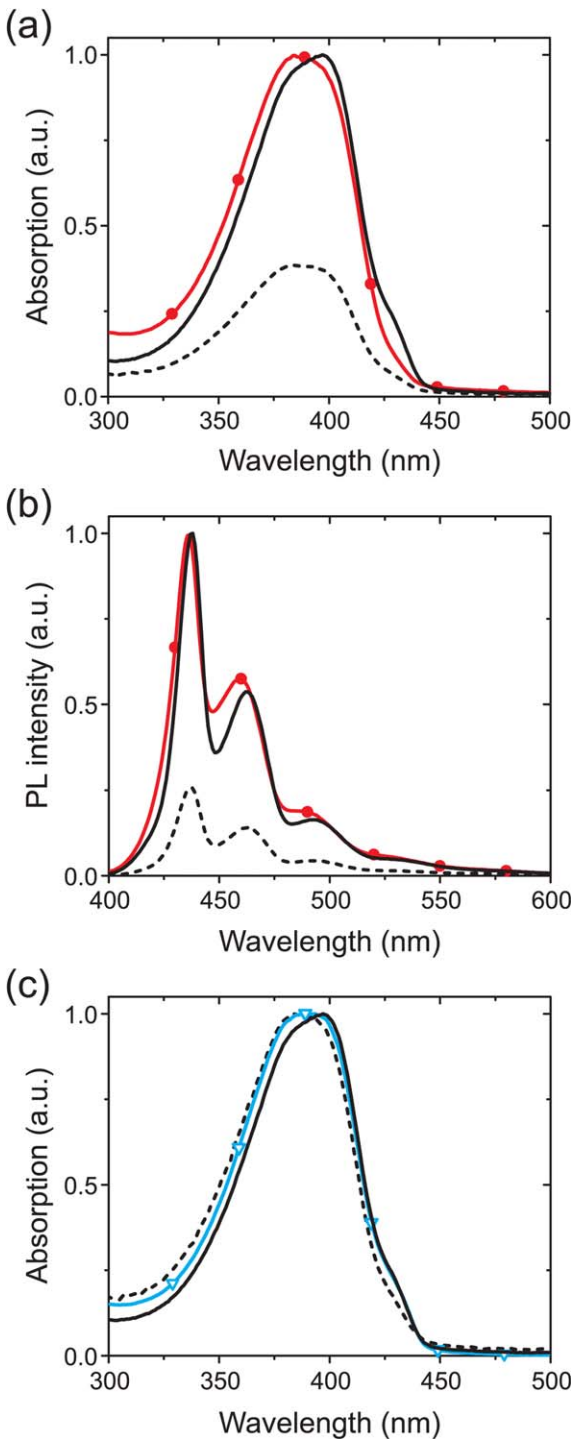

FIGURE 11 Normalized (a) absorption and (b) PL spectra of an undrawn 0.1 wt % PFO-LLDPE blend film (red line + filled circles) and the same film drawn to $\Lambda = 10$ (black lines) with the parallel- and perpendicular-polarized spectra shown by solid and dashed lines, respectively. (c) Peak-normalized polarized absorption spectra of the 0.1 wt % PFO-LLDPE blend film drawn to $\Lambda = 10$ (as above) and the absorption spectrum of an undrawn blend film subjected to the thermal protocol of drawing *without* the application of tensile stress (blue line + open triangles).

dialkylsulfide leaving groups—and leads to unexpectedly high anisotropies for modest draw ratios.[67,68]

Optical Spectroscopy of PFO-LLDPE Blend Films

Melt-processed LLDPE-PFO blends containing 0.1 wt % PFO were prepared as described in the Experimental section. The resulting films were subsequently drawn at 80 °C, above the PFO glass transition temperature, to the maximum draw ratio ($\Lambda = 10$) achievable for this LLDPE molecular weight. Absorption and PL spectra for both undrawn and drawn blend films are presented in Figure 11.

The absorption spectrum of the undrawn film shown in Figure 11(a) is reminiscent of that of crystalline PFO thin films, featuring a HOMO-LUMO absorption band with a more pronounced red-edge than that for spin-coated glassy PFO films.[4,12] Closer inspection of the spectrum, confirmed by its negative numerical second derivative,[31] also reveals the presence of a weak absorption shoulder at ~431 nm, which we attribute to absorption by crystalline PFO chains. Crystallization of PFO is expected from the sample processing history, since the blends were annealed at 230 °C, that is, within the PFO nematic melt temperature range,[2,5,12,14] followed by cooling in the cold-press. The corresponding PL spectrum, as shown in Figure 11(b), features vibronic peaks at 436, 459, and 489 nm. Its vibronic structure comprises a superposition of the PL emission spectra of (i) glassy PFO and (ii) crystalline PFO chains, consistent with the observed absorption features in Figure 11(a). Interestingly, the crystalline PL from the blend film, revealed by direct photoexcitation of crystalline chains at 432 nm, features vibronic peaks at 436, 461 and 490 nm, redshifted by ~3 nm from the corresponding vibronic positions for crystalline PFO in both melt-crystallized neat thin films[4,12] and hot-drawn PFO-UHMWPE blend films. While at this stage it is hard to unambiguously identify the origin of this redshift, it is plausibly related to crystals with longer c-axis coherence length formed as a result of either (i) the specific nucleation by LLDPE and subsequent epitaxial crystallization of PFO or (ii) crystallization occurring under strain due to material flow during melt compression molding. We note that β-phase features are absent from both absorption and PL spectra here due to the solvent-free processing of the blend film at temperatures in excess of $T_m{}^{\beta}$.

Tensile drawing of the blend film results in distinctive changes in both absorption and PL spectra as shown in Figure 11(a,b), respectively. The PL spectra are redshifted, with well-resolved vibronic peaks at 437, 462, and 493 nm for both parallel- and perpendicular-polarized spectra. The redshift and improved resolution of the spectra are due to higher PFO crystallinity in the drawn films and an associated increase in PL contribution from crystalline chains relative to glassy chains (see Fig. S7, Supporting Information for additional details). The PL emission anisotropy ratio, $R = 4$, is limited by the relatively low draw ratio of these blend films. The main absorption band in the parallel-polarized spectrum of the drawn blend film is narrowed and slightly red-shifted

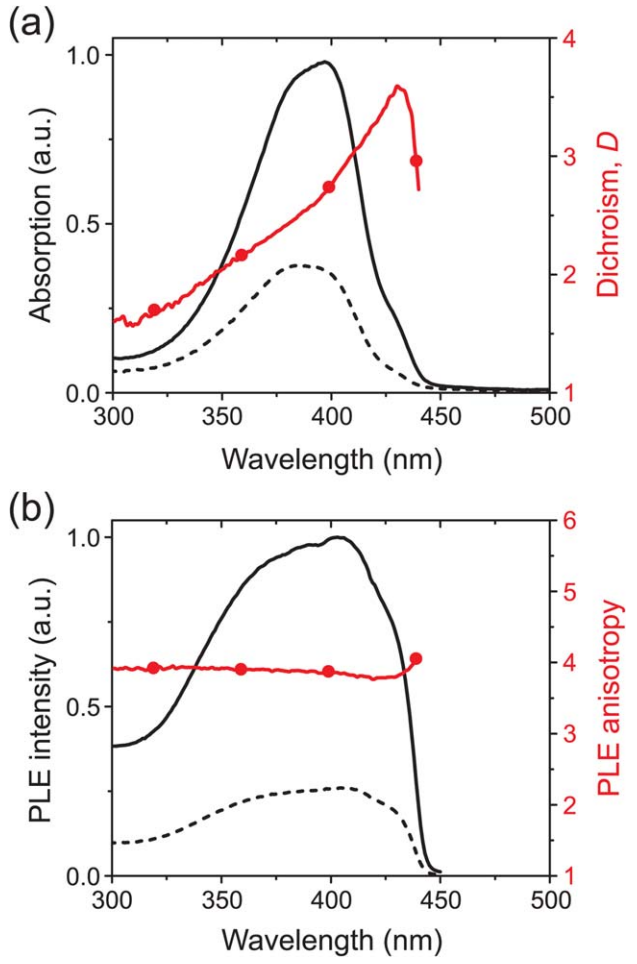

FIGURE 12 Polarized (a) absorption and (b) PLE spectra of a 0.1 wt % PFO-LLDPE blend film drawn to $\Lambda = 10$ (black lines, left ordinate) with the parallel- and perpendicular polarized spectra shown by solid and dashed lines respectively. Also shown (red lines + symbols, right ordinate) are the corresponding (a) dichroism and (b) PLE anisotropy spectra.

relative to the undrawn film. The peak absorption is at 397 nm and a significant shoulder at ~431 nm, attributed to absorption by an increased fraction of crystalline PFO chains, is seen.

With respect to PFO crystallization, tensile drawing represents a superposition of two effects, namely temperature and strain, with both influencing the crystallization behavior of the guest polymer. Figure 11(c) shows peak-normalized absorption spectra for the drawn film and a reference undrawn blend film that has been subjected to the thermal protocol of drawing but *without the application of tensile stress*. Comparison between these spectra shows that:

1. The relative magnitudes of the red-edge crystalline shoulders match for the parallel-polarized and reference film spectra because PFO crystallization takes place at the same temperature. Taking into account the fact that the absorption spectrum of the reference film also features the contribution from perpendicular oriented chains implies that the relative fraction of crystalline PFO is higher in the drawn film, consistent with strain-enhanced crystallization.
2. The main absorption bands agree more closely for the perpendicular-polarized and reference film spectra because PFO crystallization occurs in both cases under quiescent conditions, that is, without the influence of strain.

The redshift and higher relative intensity of the crystalline shoulder in the parallel-polarized absorption spectrum compared with the perpendicular-polarized spectrum confirm anisotropic crystalline chain orientation and suggest preferential crystallization of PFO along the drawing axis under applied tensile stress.

The effect that PFO crystallization under strain has on the optical anisotropy of oriented PFO-LLDPE blend films is illustrated in Figure 12. The absorption dichroism, D, calculated as the intensity ratio of parallel- and perpendicular-polarized absorption has a spectrum [see Fig. 12(a)] that peaks at 431 nm, coinciding with the spectral position of the crystalline absorption shoulder. In addition, the PLE anisotropy spectrum, monitored at 457 nm corresponding to the S_1-S_0 0-1 vibronic peak, shows the expected increase at the red-edge of the excitation spectrum. Both of these observations confirm that the PFO chains crystallized under strain exhibit a higher degree of uniaxial orientation than the majority disordered chains. Due to their more extended conjugation length and efficient excitation energy transfer from the majority, disordered chains, PL from crystalline PFO chains contributes ~90% to the overall emission spectrum. A reasonably large PL anisotropy, $R = 4$, is attained, given the modest $\Lambda = 10$ draw ratio.

Comparison of the results obtained for both UHMWPE- and LLDPE-based blends shows that PFO crystallizes during drawing in both matrix PEs. In the absence of coarse phase-separation in the undrawn films, which, as suggested by previous publications on similar blends,[47,48] can be achieved by sufficient guest dilution and melt-quench blending for UHMWPE- and LLDPE-based blends respectively, PFO chains crystallized under strain exhibit enhanced optical anisotropy compared with the glassy or β-phase chains. Regarding the β-phase, we note that the melt-based fabrication of LLDPE-PFO blend films prevents the formation of β-phase chain segments, that in oriented PFO-UHMWPE blend films are poorly aligned by drawing and consequently lead to PL emission depolarization following excitation energy transfer. Finally, the observation of a ~3 nm relative shift in PL emission from PFO chains crystallized under strain in UHMWPE- and LLDPE-based blends suggests that there may be interesting, and as yet unexplored, differences between epitaxial crystallization of PFO in the two blend types.

CONCLUSIONS

We have demonstrated that the interplay between PFO concentration and chain conformation, blend microstructure and processing conditions strongly influences the optical anisotropy of PFO in tensile-drawn gel-processed blends with UHMWPE.

A major obstacle for efficient uniaxial alignment of PFO during tensile drawing is its existence in phase-separated clusters in the undrawn blend films resulting from thermodynamic incompatibility of the two polymers. As a result, tensile stress cannot be efficiently transferred to PFO chains located within these clusters leading to their poor orientation and consequent PL emission depolarization. Reducing the concentration of PFO in the blend also reduces the size of these clusters, thus allowing for their dispersal at moderate draw ratios and subsequently enabling optimal chain alignment to occur.

Drawing at temperatures above 120 °C leads to optimal alignment of UHMWPE, with its double chain orientation signifying an extremely high degree of chain ordering. Drawing at ~65 °C leads to a less efficient orientation of the UHMWPE matrix and preserves minor regions of residual poorly oriented chains. PFO chains within these regions, consequently, also remain poorly oriented and retain a fraction of the β-phase segments found in the undrawn films. Due to their quasi-1D-crystalline structure, β-phase chain segments of PFO are erased by both (i) drawing temperatures exceeding the β-phase melting temperature of 80 °C and (ii) physical chain motion. The relationship between chain motion and the removal of the β-phase chain segments remained unclear from previous publications;[13] our results seem to confirm the link between the two processes, with the implication being that the pre-existing β-phase chain segments cannot be oriented by tensile drawing. Retaining unoriented β-phase segments in oriented PFO-UHMWPE blends leads to PL emission depolarization due to efficient exciton migration from the better-oriented, but higher HOMO-LUMO transition energy, glassy, and crystalline chain segments.

With regards to the drawing method, we have determined that maintaining constant *elongation* rather than *strain* rate during drawing results in less efficient guest alignment due more preferential chain relaxation at high draw ratios.

We have also observed that PFO crystallization occurs during tensile drawing. Following dispersal of phase-separated PFO clusters, the crystallized PFO chain segments are closely aligned with the drawing axis as a result of their crystallization taking place under strain. Due to their extended conformation and, hence, a lower energy electronic state relative to glassy chains, PL emission occurs preferentially from the crystalline chain segments, yielding optimal PL emission anisotropy for these blends. The chemical similarity between PE and the alkyl side-chains of PFO may enable side-chain-driven epitaxial crystallization of PFO to occur.

In addition, melt-processed PFO-LLDPE blends were fabricated and characterized for the first time. Due to the melt-based fabrication, no β-phase chain segments survive here and the PFO chains are more-optimally dispersed in the undrawn blend films, leading to efficient orientation during tensile drawing. Finally, our findings for crystallization of PFO during tensile drawing of these melt-processed PFO-LLDPE films are fully consistent with the corresponding observations for gel-processed PFO-UHMWPE blends.

ACKNOWLEDGMENTS

The authors thank the UK Engineering and Physical Sciences Research Council (grant EP/H000917/1) and the IDEA League for financial support. They also thank the Sumitomo Chemical Company Ltd for supplying the PFO polymer used in this study and David James and Ji-Seon Kim (Centre for Plastic Electronics, Imperial College London) for assistance with Raman spectroscopy measurements. A. Perevedentsev thanks the Polymer Technology group at the Department of Materials, ETH Zürich, for hosting his research visit and providing access to the stimulating environment of Geordies' where many of the presented ideas were engendered. D.D.C. Bradley is the Lee-Lucas Professor of Experimental Physics.

REFERENCES AND NOTES

1 J. H. Burroughes, D. D. C. Bradley, A. R. Brown, R. N. Marks, K. D. Mackay, R. H. Friend, P. L. Burn, A. B. Holmes, *Nature* **1990**, *347*, 539–541.

2 M. Grell, D. D. C. Bradley, G. Ungar, J. Hill, K. Whitehead, *Macromolecules* **1999**, *32*, 5810–5817.

3 M. Ariu, D. G. Lidzey, D. D. C. Bradley, *Synth. Met.* **2000**, *111*, 607–610.

4 M. Ariu, D. G. Lidzey, M. Sims, A. J. Cadby, P. A. Lane, D. D. C. Bradley, *J. Phys.: Condens. Matter* **2002**, *14*, 9975–9986.

5 M. Sims, K. Zheng, M. Campoy-Quiles, R. Xia, P. N. Stavrinou, D. D. C. Bradley, P. Etchegoin, *J. Phys.: Condens. Matter* **2005**, *17*, 6307–6318.

6 T. Kreouzis, D. Poplavskyy, S. M. Tuladhar, M. Campoy-Quiles, J. Nelson, A. J. Campbell, D. D. C. Bradley, *Phys. Rev. B* **2006**, *73*, 235201.

7 D. D. C. Bradley, M. Grell, X. Long, H. Mellor, A. W. Grice, M. Inbasekaran, E. P. Woo, *SPIE Proc.* **1997**, *3145*, 254–259.

8 A. J. Cadby, P. A. Lane, H. Mellor, S. J. Martin, M. Grell, C. Giebeler, D. D. C. Bradley, M. Wohlgenannt, C. An, Z. V. Vardeny, *Phys. Rev. B* **2000**, *62*, 15604–15609.

9 M. Ariu, M. Sims, M. D. Rahn, J. Hill, A. M. Fox, D. G. Lidzey, M. Oda, J. Cabanillas-Gonzalez, D. D. C. Bradley, *Phys. Rev. B* **2003**, *67*, 195333.

10 G. Ryu, P. N. Stavrinou, D. D. C. Bradley, *Adv. Funct. Mater.* **2009**, *19*, 3237–3242.

11 W. Chunwaschirasiri, B. Tanto, D. L. Huber, M. J. Winokur, *Phys. Rev. Lett.* **2005**, *94*, 107402.

12 S. H. Chen, A. C. Su, C. H. Su, S. A. Chen, *Macromolecules* **2005**, *38*, 379–385.

13 S. H. Chen, A. C. Su, S. A. Chen, *J. Phys. Chem. B* **2005**, *109*, 10067–10082.

14 M. Grell, D. D. C. Bradley, M. Inbasekaran, E. P. Woo, *Adv. Mater.* **1997**, *9*, 798–802.

15 M. Grell, D. D. C. Bradley, X. Long, T. Chamberlain, M. Inbasekaran, E. P. Woo, M. Soliman, *Acta Polym.* **1998**, *49*, 439–444.

16 M. Redecker, D. D. C. Bradley, M. Inbasekaran, E. P. Woo, *Appl. Phys. Lett.* **1999**, *74*, 1400–1402.

17 K. S. Whitehead, M. Grell, D. D. C. Bradley, M. Jandke, P. Strohriegl, *Appl. Phys. Lett.* **2000**, *76*, 2946–2948.

18 A. R. Buckley, M. D. Rahn, J. Hill, J. Cabanillas-Gonzalez, A. M. Fox, D. D. C. Bradley, *Chem. Phys. Lett.* **2001**, *339*, 331–336.

19 T. Virgili, D. Marinotto, G. Lanzani, D. D. C. Bradley, *Appl. Phys. Lett.* **2005**, *86*, 091113.

20 T. A. M. Ferenczi, M. Sims, D. D. C. Bradley, *J. Phys.: Condens. Matter* **2008**, *20*, 045220.

21 A. Asimakis, PhD Thesis, Imperial College London, **2005**.

22 T. Endo, T. Kobayashi, T. Nagase, H. Naito, *Thin Solid Films* **2008**, *517*, 1324–1326.

23 M. Misaki, Y. Ueda, S. Nagamatsu, Y. Yoshida, N. Tanigaki, K. Yase, *Macromolecules* **2004**, *37*, 6926–6931.

24 T. Kawamura, M. Misaki, Y. Koshiba, S. Horie, K. Kinashi, K. Ishida, Y. Ueda, *Thin Solid Films* **2011**, *519*, 2247–2250.

25 M. Brinkmann, *Macromolecules* **2007**, *40*, 7532–7541.

26 M. Misaki, M. Chikamatsu, Y. Yoshida, R. Azumi, N. Tanigaki, K. Yase, S. Nagamatsu, Y. Ueda, *Appl. Phys. Lett.* **2008**, *93*, 023304.

27 R. Xia, M. Campoy-Quiles, G. Heliotis, P. N. Stavrinou, K. S. Whitehead, D. D. C. Bradley, *Synth. Met.* **2005**, *155*, 274–278.

28 T. Virgili, D. G. Lidzey, M. Grell, S. Walker, A. Asimakis, D. D. C. Bradley, *Chem. Phys. Lett.* **2001**, *341*, 219–224.

29 M. Campoy-Quiles, P. G. Etchegoin, D. D. C. Bradley, *Phys. Rev. B* **2005**, *72*, 045209.

30 T. W. Hagler, H. Pakbaz, J. Moulton, F. Wudl, P. Smith, A. J. Heeger, *Polym. Commun.* **1991**, *32*, 339–342.

31 T. W. Hagler, H. Pakbaz, K. F. Voss, A. J. Heeger, *Phys. Rev. B* **1991**, *44*, 8652–8666.

32 S. M. King, H. L. Vaughan, A. P. Monkman, *Chem. Phys. Lett.* **2007**, *440*, 268–272.

33 H. L. Vaughan, A. P. Monkman, L. O. Palsson, B. S. Nehls, T. Farrell, U. Scherf, *J. Chem. Phys.* **2008**, *128*, 044709.

34 C. Weder, C. Sarwa, A. Montali, C. Bastiaansen, P. Smith, *Science* **1998**, *279*, 835–837.

35 A. Montali, C. Bastiaansen, P. Smith, C. Weder, *Nature* **1998**, *392*, 261–264.

36 C. Weder, C. Sarwa, C. Bastiaansen, P. Smith, *Adv. Mater.* **2004**, *9*, 1035–1039.

37 P. Smith, P. J. Lemstra, *Colloid Polym. Sci.* **1980**, *258*, 891–894.

38 P. Smith, P. J. Lemstra, H. C. Booij, *J. Polym. Sci. Polym. Phys. Ed.* **1981**, *19*, 877–888.

39 P. Smith, P. J. Lemstra, J. P. L. Pijpers, A. M. Kiel, *Colloid Polym. Sci.* **1981**, *259*, 1070–1080.

40 B. Q. He, J. Li, Z. Bo, Y. Huang, *Macromolecules* **2005**, *38*, 6762–6766.

41 M. Knaapila, H. L. Vaughan, T. P. A. Hase, R. C. Evans, R. Stepanyan, M. Torkkeli, H. D. Burrows, U. Scherf, A. P. Monkman, *Macromolecules* **2010**, *43*, 299–305.

42 M. Sims, D. D. C. Bradley, M. Ariu, M. Koeberg, A. Asimakis, M. Grell, D. G. Lidzey, *Adv. Funct. Mater.* **2004**, *14*, 765–781.

43 E. J. W. List, R. Guentner, P. S. de Freitas, U. Scherf, *Adv. Mater.* **2002**, *14*, 374–378.

44 K. Becker, J. M. Lupton, K. Feldmann, B. S. Nehls, F. Galbrecht, D. Gao, U. Scherf, *Adv. Funct. Mater.* **2005**, *16*, 364–370.

45 K. L. Chan, M. Sims, S. I. Pascu, M. Ariu, A. B. Holmes, D. D. C. Bradley, *Adv. Funct. Mater.* **2009**, *19*, 2147–2154.

46 B. Q. He, C. Wu, Y. Huang, *Macromol. Chem. Phys.* **2007**, *208*, 384–388.

47 M. Eglin, A. Montali, A. R. A. Palmans, T. Tervoort, P. Smith, C. Weder, *J. Mater. Chem.* **1999**, *9*, 2221–2226.

48 A. Montali, A. R. A. Palmans, M. Eglin, C. Weder, P. Smith, W. Trabesinger, A. Renn, B. Hecht, U. P. Wild, *Macromol. Symp.* **2000**, *154*, 105–116.

49 J. R. Lakowicz, In Principles of Fluorescence Spectroscopy, 2nd ed.; Plenum: New York, **1999**.

50 A. L. T. Khan, P. Sreearunothai, L. M. Herz, M. Banach, A. Köhler, *Phys. Rev. B* **2004**, *69*, 085201.

51 J. Peet, E. Brocker, Y. Xu, G. C. Bazan, *Adv. Mater.* **2008**, *20*, 1882–1885.

52 G. Ryu, R. Xia, D. D. C. Bradley, *J. Phys.: Condens. Matter* **2007**, *19*, 056205.

53 X. Long, A. Malinowski, D. D. C. Bradley, M. Inbasekaran, E. P. Woo, *Chem. Phys. Lett.* **1997**, *272*, 6–12.

54 M. Grell, D. D. C. Bradley, *Adv. Mater.* **1999**, *11*, 895–905.

55 Y. Termonia, S. R. Allen, P. Smith, *Macromolecules* **1988**, *21*, 3485–3489.

56 M. Matsuo, R. St. J. Manley, *Macromolecules* **1982**, *15*, 985–987.

57 H. Liem, P. Etchegoin, K. S. Whitehead, D. D. C. Bradley, *Adv. Funct. Mater.* **2003**, *13*, 66–72.

58 M. C. Gather, D. D. C. Bradley, *Adv. Funct. Mater.* **2007**, *17*, 479–485.

59 W. F. Wong, R. J. Young, *J. Mater. Sci.* **1994**, *29*, 510–519.

60 S. Heun, R. F. Mahrt, A. Greiner, U. Lemmer, H. Bässler, D. A. Halliday, D. D. C. Bradley, P. L. Burn, A. B. Holmes, *J. Phys.: Condens. Matter* **1993**, *5*, 247–260.

61 K. Ishikawa, K. Miyasaka, M. Maeda, *J. Polym. Sci. Part A-2: Polym. Phys.* **1969**, *7*, 2029–2041.

62 B. Schartel, V. Wachtendorf, M. Grell, D. D. C. Bradley, M. Hennecke, *Phys. Rev. B* **1999**, *60*, 277–283.

63 J. H. Chen, C. S. Chang, Y. X. Chang, C. Y. Chen, H. L. Chen, S. A. Chen, *Macromolecules* **2009**, *42*, 1306–1314.

64 M. Knaapila, A. P. Monkman, *Adv. Mater.* **2013**, *25*, 1090–1108.

65 A. R. A. Palmans, M. Eglin, A. Montali, C. Weder, P. Smith, *Chem. Mater.* **2000**, *12*, 472–480.

66 M. Campoy-Quiles, M. Sims, P. G. Etchegoin, D. D. C. Bradley, *Macromolecules* **2006**, *39*, 7673–7680.

67 D. D. C. Bradley, R. H. Friend, H. Lindenberger, S. Roth, *Polymer* **1986**, *27*, 1709–1713.

68 D. D. C. Bradley, *J. Phys. D: Appl. Phys.* **1987**, *20*, 1389–1410.